Shock Wave Induced Decomposition Chemistry of Pentaerythritol Tetranitrate Single Crystals: Time-Resolved Emission Spectroscopy

Zbigniew A. Dreger, Yuri A. Gruzdkov, and Yogendra M. Gupta*

Institute for Shock Physics and Department of Physics, Washington State University, Pullman, Washington 99164-2816

Jerry J. Dick

MS P952, Los Alamos National Laboratory, Los Alamos, New Mexico 87545

Received: May 3, 2001; In Final Form: October 25, 2001

The decomposition mechanism in shocked pentaerythritol tetranitrate (PETN) was examined using time-resolved emission spectroscopy. PETN single crystals were subjected to stepwise loading along [100] and [110] to peak stresses between 2 and 13 GPa. Due to concurrent changes in the optical transmission of PETN, emission spectra were analyzed using the absorption data acquired separately under the same loading conditions. Analyses of the corrected emission data revealed two bands in the spectra at ∼3.0 and ∼2.4 eV. Both bands were observed in every experiment regardless of stress or crystal orientation. However, their relative and absolute intensities, and temporal behavior revealed stress and orientation dependence. The emission was identified as chemiluminescence from the nitronium ion, NO_2^+, on the basis of its electronic structure and properties. NO_2^+ electronic structure was analyzed using ab initio calculations, which showed transition energies matching those of the emitting intermediate observed experimentally. Several chemical pathways compatible with the formation of NO_2^+ are considered and evaluated. Finally, a four-step chemical initiation mechanism in shocked crystalline PETN is proposed and discussed in detail.

I. Introduction

Understanding decomposition mechanisms associated with shock initiation of high explosives (HE) is important for improvements in HE performance and for mitigation of hazards in storage and handling. For these reasons, shock initiation of HEs has received much attention in the past.[1] Although the macroscopic (thermal and mechanical) behavior of HEs has been examined extensively, chemical decomposition mechanisms under shock loading are not well understood. A combination of continuum measurements (pressure, particle velocity) and time-resolved spectroscopic methods is needed to provide the necessary macroscopic and microscopic insight into this challenging problem.[2] This combined approach is particularly important for solid HEs where the mechanical response and initiation chemistry are strongly coupled.[3−5]

In this work, we sought to characterize the decomposition mechanism in single crystals of pentaerythritol tetranitrate (PETN, 1,3-propanediol, 2,2-bis(nitroxy)methyl-, dinitrate (ester)). Use of single crystals avoids the inherent complexities in the mechanical response of inhomogeneous solid materials, such as powders and composites, and is desirable for fundamental studies. PETN is a crystalline HE used extensively as an ingredient in many explosive formulations. Previous work on PETN has concentrated primarily on its mechanical response[4,6] and the shock to detonation transition (SDT).[7,8] The time and run distance to detonation in PETN crystals depends strongly on the orientation along which the crystal is shocked. Also, it was found that along the [110] orientation, crystals are more sensitive near 4.2 GPa than at 8.5 GPa.[6,9−11] The observed anisotropy and the SDT anomaly for the [110] orientation are not well understood.[5,12,13] Strong light emission accompanying the changes in PETN was observed when the crystal was shocked along the [110] and [001] orientations.[4,6,14,15] Based on available data, this emission was tentatively assigned to chemiluminescence associated with PETN decomposition in the early stages of initiation.[4] An accurate determination of the origin of the emission was not possible due to the limited amount of data,[4] the lack of time-resolved measurements, and the needed complimentary absorption data.[16] Consequently, the decomposition chemistry responsible for emission could not be determined.

In the present work, we address the deficiencies indicated in prior studies by fully characterizing light emission from shocked PETN. Among the new features introduced in this work are time-resolved emission measurements and analytical corrections of the emission spectra due to concurrent changes in absorption of shocked PETN. Furthermore, our experiments are designed to explore the possibility of using this emission to identify chemical changes to the sample. The results are analyzed using ab initio computational methods.

The remainder of this paper is organized as follows. Sample preparation and experimental techniques are described in the next section. Section III presents the experimental results, covering both absorption and emission measurements. In section IV, we discuss the origin of the emission, identify the emitting intermediate, and propose a plausible reaction mechanism in shocked PETN. The main findings of this work are summarized in section V.

II. Experimental Methods

A. Sample Preparation. The PETN single crystals used in these studies were grown at Los Alamos National Laboratory as described in ref 17. The samples were optically clear and

10.1021/jp011682v CCC: $22.00
Published on Web 12/12/2001

contained less than 100 ppm of organic impurities as indicated by NMR and chromatography. The crystals were cut using a diamond saw into thin (ca. 1 mm) slabs with either the [110] or [100] crystal axis orthogonal to the face of the slab. The crystal orientation was maintained to better than 1 degree. The slabs were cleaved into smaller pieces, typically rectangular in shape, with lateral dimensions of approximately 8−10 mm. Each piece was ground down and polished using a progression of aluminum oxide lapping sheets (30, 10, 1, and 0.3 micron, Fiber Optics Center, MA) and an aqueous solution of detergent as a lubricant. This procedure resulted in optically clear crystal slides with a thickness from 350 to 500 μm. Typically, the thickness across the sample was maintained to better than 5 μm and the surfaces were flat to ca. 5 wavelengths of visible light.

In all emission and absorption experiments, the PETN slides were sandwiched between two LiF windows. The front and back windows were 25.4 and 19 mm in diameter and 3 and 5 mm in thickness, respectively. The sample was centered on the windows using a plastic mask cut to the exact shape of the sample. Liquid glycerol (spectrophotometric grade, 99.5+%, Aldrich Chemical) was used to fill the small (<4 μm) gaps between the sample and windows. In a separate set of control experiments, we verified that glycerol remains optically transparent and chemically inert under the loading conditions of interest.

B. Impact Experiments. Shock waves were generated by impacting a piece of *a*-cut sapphire mounted on a projectile onto the LiF front window of a sample cell. The projectile was accelerated to the desired velocity using a single-stage light-gas gun.[18] After traversing the front window, the shock wave reverberated between the windows bringing the PETN sample to the final stress and temperature in approximately three steps and 300 ns. The lateral dimensions of the sample allowed for at least 800-ns recording time, after the entry of the shock wave in the sample, before release waves arrived from the sample edges. Stress histories in the sample in each experiment were calculated using a one-dimensional wave propagation code, COPS.[19] The calculations used a material model describing the shock response of sapphire,[20] LiF,[21] and PETN. The latter is currently under development in our laboratory.[22] Experimental details are summarized in Table 1.

Emission Measurements. Light emitted from shocked PETN was collected as illustrated schematically in Figure 1. The light was delivered through optical fibers (400 μm core diameter) to a fast photodiode (DET2-SI, Thorlabs) and to the spectral detection system shown in Figure 1. The output of the spectrometer (SpectraPro-150, Acton Research Corporation) was dispersed temporally (~50 ns resolution) by an electronic streak camera (Imacon 500, Hadland) producing a two-dimensional image (intensity vs time vs wavelength) on the phosphor screen of the streak camera. This image was amplified by a micro-channel plate intensifier and recorded by a CCD detector (PI CCD, 1024 × 1024 back-illuminated chip). The photodiode signal at a 4-ns sampling rate was used as an overall intensity monitor and a timing diagnostic. Although both sets of data can be recorded with higher time resolution, the higher resolution was not needed in this work.

All emission experiments, except for experiments E9 and E11, were performed in the configuration described above. We refer to this configuration as the standard configuration. Experiments E9 and E11 were carried out in a configuration that we refer to as the reverse configuration. In contrast to the standard configuration, the sample assembly in the reverse configuration is mounted on a projectile and impacted onto a stationary sapphire piece. The configurations are compared in Figure 2. In the reverse configuration, the signal is collected through the sapphire and in a direction that is opposite to the initial shock propagation direction. The reasons for using the reverse configuration are discussed in section III.

TABLE 1: List of Experiments

expt	crystal orientation	sample thickness (μm)	projectile velocity (km/s)	calc. final stress (GPa)
		absorption		
A1 (99−021)	[100]	400	0.860	10.1
A2 (98−050)	[100]	375	0.669	7.7
A3 (98−046)	[100]	460	0.454	5.1
A4 (98−051)	[100]	475	0.253	2.7
A5 (99−022)	[110]	405	0.879	10.4
A6 (99−014)	[110]	400	0.656	7.5
A7 (99−007)	[110]	460	0.442	4.9
A8 (99−028)	[110]	475	0.211	2.3
		emission		
E1 (99−017)	[100]	430	0.855	10.0
E2 (99−015)	[100]	420	0.661	7.6
E3 (98−044)	[100]	405	0.453	5.1
E4 (98−048)	[100]	400	0.207	2.2
E5 (99−060)	[110]	380	1.08	13.0
E6 (99−016)	[110]	420	0.852	9.7
E7 (98−053)	[110]	415	0.667	7.7
E8 (99−027)	[110]	805	0.653	7.5
E9 (99−059)[a]	[110]	410	0.652	7.5
E10 (98−049)	[110]	440	0.449	5.0
E11 (99−006)[a]	[110]	410	0.445	5.0
		scattering		
S1 (99−031)[b]	[100]	380	0.320	2.5

[a] Reverse configuration. [b] LiF impactor and *z*-cut quartz windows were used.

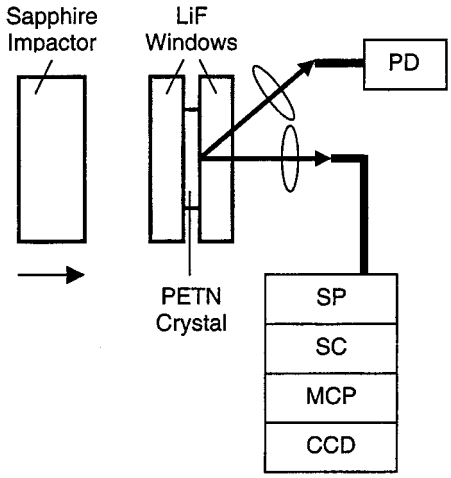

Figure 1. Schematic diagram of the experimental configuration. Shock waves are launched by impact between a sapphire impactor and the front window of the sample cell. Light emitted from the shocked PETN crystal is collected into an optical fiber and delivered to the detection system consisting of a spectrometer (SP), streak camera (SC), micro-channel plate (MCP), and charge coupled detector (CCD). Temporal profile of the emission is recorded by a fast photodiode (PD).

To obtain true emission spectra, the recorded spectra were first corrected for the spectral response of the detection system. This was accomplished by calibrating the spectral sensitivity of the entire system (collection, dispersion, and acquisition combined) using a tungsten-filament quartz halogen lamp (EN-101, Eppley) as a standard light source. The instrumental correction function or spectral response, $C(\lambda)$, was determined as a ratio of intensities of the tabulated source spectrum provided by the lamp manufacturer and the same spectrum measured

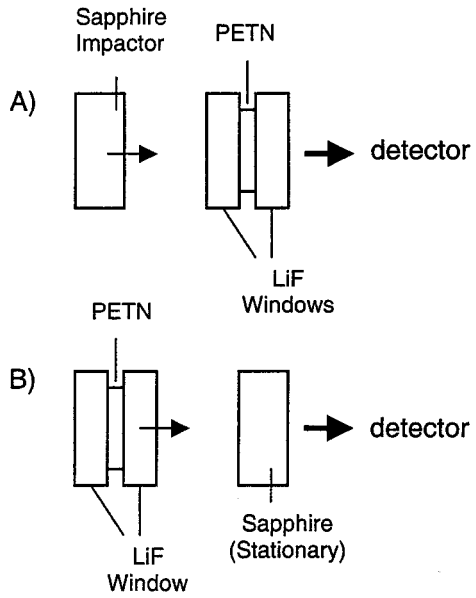

Figure 2. Experimental configurations: (A) standard, (B) reverse. The sizes of the crystal and windows are not drawn to scale.

using our detection system. This function was consequently used to correct the experimental data.

In addition to the instrumental correction, an additional correction to the data was necessary since the shocked PETN absorbs light quite strongly.[23] Therefore, light attenuation inside the sample had to be taken into account. The latter required knowledge of the light extinction in the sample, which had to be measured separately. Further details about this correction are given in section III B.

Absorption Measurements. For each emission experiment, a matching extinction experiment was performed (see Table 1). The configuration for time-resolved extinction measurements was similar to that used in our earlier work.[24,25] A pulsed xenon flashlamp was used as the light source. The output was filtered, collimated, and directed through the sample. The transmitted light was delivered to a streak camera/spectrometer/CCD system that recorded time-resolved transmission spectra with 50 ns time resolution. These spectra were then converted to extinction data as described in ref 26.

Since two different physical processes, absorption and scattering, could cause light extinction in the sample, we used a separate experiment to determine directly the possible contribution of scattering from the sample. A beam of laser light (514.5 nm) was sent through the PETN sample along its normal, and the elastically scattered light was collected at 45 degrees to the normal in a backscattering geometry. The intensity of the scattered light was monitored using a fast photodiode.[23] *Z*-cut quartz windows were used in the scattering experiment because quartz remains elastic up to 6 GPa.[27] The elastic response of the quartz windows eliminates any potential contribution to the scattering signal from the windows. The result of this experiment is presented in section III A.

As indicated in Table 1, a total of 20 experiments (11 emission, 8 absorption, and 1 scattering) were carried out in this work. The final stress in the PETN sample in each of the experiments could be determined very accurately (within 1−2%) because this stress is related only to the projectile velocity and the known shock response of the impactor and windows.[20,21,27] To support the emission data analyses, the same loading conditions were employed in emission and extinction experiments.

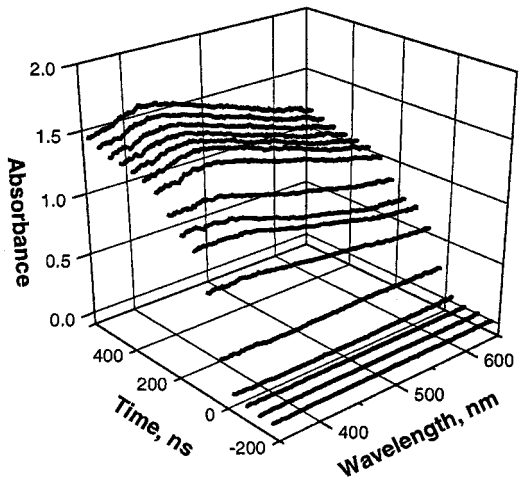

Figure 3. Time-resolved absorption spectra of PETN shocked to 5.1 GPa along the [100] direction (experiment A3). At 0 ns shock enters the sample.

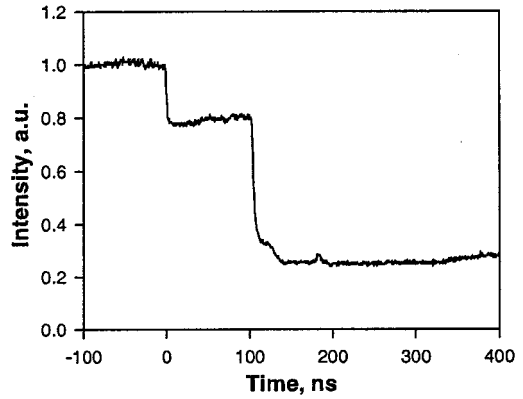

Figure 4. Intensity of scattered light at 514 nm as a function of time. PETN is shocked along the [100] direction to a final stress of 2.5 GPa. At 0 ns shock enters the sample; at 100 ns the shock wave hits the sample/back window interface.

III. Results

A. Absorption. At ambient pressure, the UV−vis absorption spectrum of PETN consists of three bands: 193.5, 260, and 290 nm. The corresponding transitions are all localized on the $-NO_2$ groups of PETN and have been assigned to $\pi \rightarrow \pi^*$, $n \rightarrow \pi^*$, and $n \rightarrow \pi^*$ transitions, respectively.[28] Within the spectral range accessible to us, only the band edge of the 290-nm band could be seen at ca. 310 nm. Samples were transparent above 310 nm. Absorption spectra for a typical experiment are shown in Figure 3.

As seen in Figure 3, after the shock wave enters PETN a very broad featureless absorption band in the visible begins to grow. Four experiments at different final stresses (ca. 2.5, 5, 7.5, and 10 GPa) were performed for each of the [110] and [100] orientations. These experiments provided the time-resolved absorption data necessary for proper analysis of the emission data.

In a control scattering experiment (S1, Table 1), we verified that light attenuation in shocked PETN is caused by absorption and not by scattering. The result of this experiment is shown in Figure 4. The initial scattering signal ($t < 0$) originated from the two sample/window interfaces and small imperfections on the sample surface. Its intensity was 6 to 7 orders of magnitude less than the excitation laser beam intensity. When the shock wave reached the front interface at $t = 0$, it compressed the gap, reducing the amount of scattering. From 0 to 100 ns, the

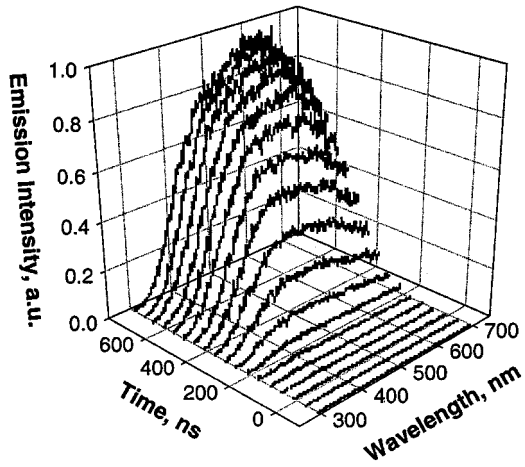

Figure 5. Time-resolved emission spectra of PETN shocked to 7.6 GPa along the [100] direction (experiment E2). The spectra have been corrected for the detector sensitivity. At 0 ns shock enters the crystal; by ~350 ns the final stress is reached. Spectra were taken with 50 ns resolution.

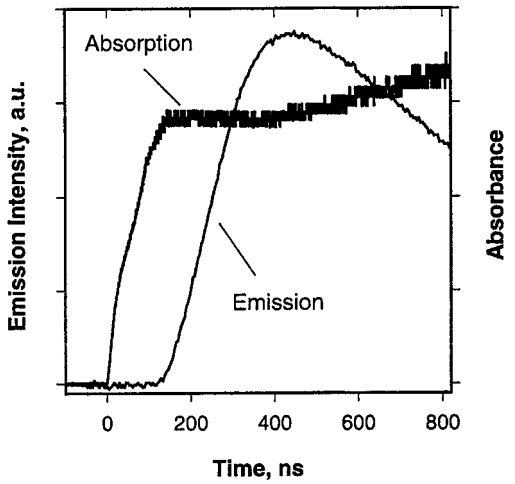

Figure 6. Temporal profiles of absorption and emission. The curves represent photodiode records for experiments A6 and E7. Shock enters the samples at 0 ns.

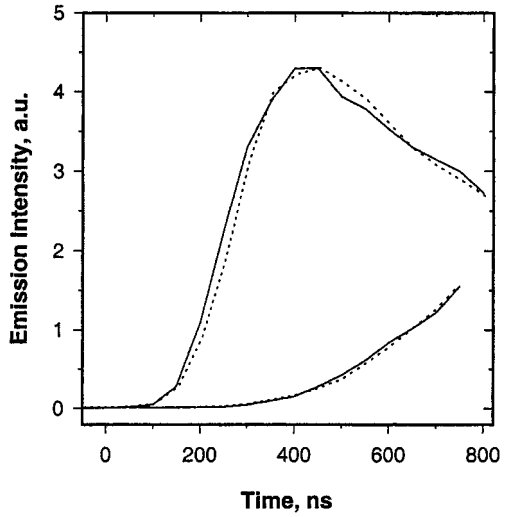

Figure 7. Temporal profiles of emission for the standard (solid line) and reverse (dotted line) configuration. The following experiments are compared: E10 and E11 (5 GPa, low emission intensity), E7 and E9 (~7.6 GPa, high emission intensity). Shock enters the sample at 0 ns.

shock wave traversed the sample. Effectively, there was no change in scattering during that time interval while transmission through the sample was decreasing by ca. 60% (prior measurement). When the shock wave reached the back interface, the scattering signal decreased sharply again due to compression of the back interface. After that, there was no further change in scattering while transmission through the sample kept decreasing down to a few percent. From the result in Figure 4, we concluded that light attenuation observed in extinction experiments was indeed due to absorption; the contribution of scattering did not exceed 0.001% and could be ignored for all practical purposes. Since the experiment revealed no scattering, the terms "absorption" and "extinction" can be used interchangeably in the present work.

The observed absorption in shocked PETN is not fully understood at the present time. The subnanosecond time scale of the process causing absorption may indicate an electronic process, such as stress or deformation induced change of the electronic band structure of PETN.[23,29]

B. Emission. Light emission from both the [110] and [100] orientations of PETN was observed when the crystal was subjected to stepwise shock loading with final stresses as low as 5 GPa; the precise lower limit was not established. There was no emission at 2.2 GPa for the [100] orientation (experiment E4). In previous studies,[4,14,15] light emission was observed only for crystals shocked along the [110] and [001] directions; no emission was found for the [100] crystal orientation. The apparent discrepancy with our results is most likely due to the lower sensitivity of the previous detection systems.

Typical time-resolved emission spectra of shocked PETN (experiment E2) are shown in Figure 5. As can be seen, the emission covers a broad spectral range from 300 to beyond 700 nm (700 nm was the long wavelength limit of our detection system). The emission onset occurs at ~150 ns and the emission intensity increases while the shock wave is still reverberating in the sample. It continues to increase after the final stress is reached at ~300 ns.

As discussed in the preceding section, shocked PETN absorbs light throughout the entire visible range. Because this absorption overlaps spectrally and temporally with the emission, the latter is attenuated before the radiation exits the sample. Therefore, to obtain true emission spectra, the recorded spectra must be corrected for light reabsorption in PETN. To implement this correction one must know the spatial distribution of the emitting and absorbing species across the sample (see Appendix). Experimental or theoretical determination of the spatial distributions is a complex problem since a shock wave constitutes a moving discontinuity. Hence, no two locations inside the sample will have the same history of stress and temperature. The resulting spatial distributions of the absorbing/emitting species will reflect the time-dependent processes that give rise to absorption/emission and the history of these changes in the shocked sample.

Despite this complexity, some qualitative conclusions could still be drawn from the data presented in Figures 6 and 7. Figure 6 compares the temporal profiles of absorption (Exp. A6) with emission (Exp. E7) that are typical for the set of experiments presented here. It indicates that at the onset of emission the absorbance has already reached a plateau. Further absorption changes are fairly small and slow for the entire duration of emission. This behavior implies that the absorbing species has attained a steady state across the sample and the spatial distribution is close to uniform.

Figure 7 compares emission results obtained in the standard and reverse configurations (see Figure 2). It has been suggested

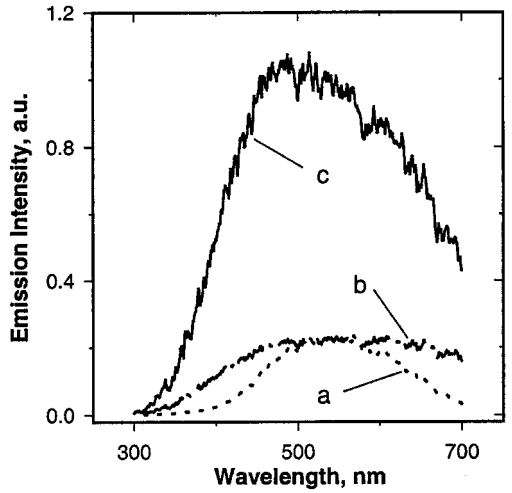

Figure 8. Result of corrections for a typical emission spectrum: (a) recorded spectrum, (b) after instrumental ($C(\lambda)$) correction only, (c) after applying eq 1.

that the emitting region may be narrow and concentrated near the shock front.[4] In such a scenario, emission signals should be different in these two configurations since the emitted light has to travel different optical paths to reach the detector. On the other hand, if the emitting region is broad and includes the entire shocked sample, the difference between the two configurations should be small. Figure 7 shows that the emission traces coincide almost exactly, indicating the broad spatial distribution.

Based on the data and arguments presented above, we assumed that both the emitting and absorbing species are distributed uniformly in the bulk of shocked PETN. With this assumption, an expression for "true emission", $I_T(\lambda, t)$, can be easily derived (see Appendix):[30]

$$I_T(\lambda,t) = \frac{A(\lambda,t)I_R(\lambda,t)\ln 10}{C(\lambda)(1 - 10^{-A(\lambda,t)})} \quad (1)$$

where $C(\lambda)$ is the spectral response of the detection system, $I_R(\lambda, t)$ is the recorded emission intensity, and $A(\lambda, t)$ is the measured absorbance of the sample. Figure 8 shows the effect of the corrections on a typical emission spectrum acquired using our detection system. It is seen that the spectrum becomes broader and shifts to higher energies. All the data presented below have been corrected using eq 1.

As indicated, emission appears after an induction period of at least 100 ns relative to when the shock wave enters the sample. The results in Figure 9 demonstrate that the induction period depends on both the crystal orientation and the final stress in the sample. The traces shown were obtained from emission spectra by integrating the area under the curve from 300 to 700 nm. In general, the induction periods are shorter for the [110] orientation than for the [100] orientation. Also, the effect of stress on the induction period is different for the two orientations. For the [100] orientation, the induction period decreases monotonically as the stress increases. In contrast, it goes through a local minimum at 7.7 GPa (final stress) for the [110] orientation.

Emission spectra change significantly with time and/or stress. However, both crystallographic orientations produce very similar spectral features. As illustrated in Figure 10, the spectral shape of the emission shows a tendency to broaden and to shift to lower energies with time. Analysis of this spectral evolution reveals that the spectra consist of two components that can be fitted well by Gaussian peaks. The first component is the high-

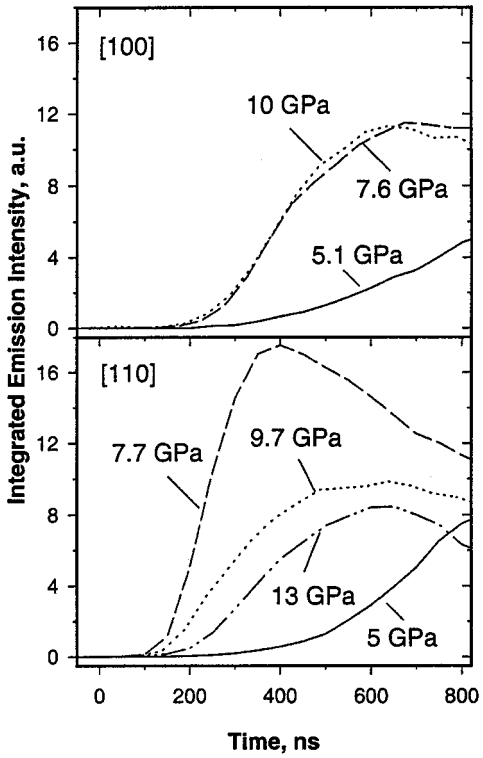

Figure 9. Temporal profile of global emission intensity from PETN shocked along two different crystallographic directions. Shock direction and final stress values are shown. Time resolution is 50 ns; shock enters the sample at 0 ns.

energy band (HEB) located at ~3.0 eV, which emerges first. The second component, low-energy band (LEB), located at ~2.4 eV, appears ~50 ns later. Intensity of the LEB grows faster than the HEB, with both bands shifting gradually to lower energies as time progresses. However, the observed separation between the bands, ~0.6 eV, appears to be constant regardless of the shift. This behavior is illustrated in Figure 11.

The absolute and relative intensities, and the positions of the low and high-energy bands also change with stress, as shown in Figure 12. Similar to the induction period, the absolute intensity of both bands goes through an extremum at 7.7 GPa for the [110] orientation. However, the intensity ratio of the LEB to the HEB increases continuously with stress. At high stresses, the emission becomes dominated by the LEB.

IV. Discussion

A. Origin of Emission. Light emission occurring in shocked PETN can arise from three potential sources: (i) thermal emission, (ii) electronically excited PETN molecules, or (iii) excited intermediates. Several factors suggest that the observed emission cannot arise from thermal emission. First, the emission appears at stresses as low as 5 GPa. The estimated temperature increase in PETN at this stress is on the order of 100 K,[22] which is not sufficient to produce thermal emission in the visible. Furthermore, the emission spectra cannot be fitted satisfactorily to Wien's law. Finally, the maximum of the emission spectrum (at 5 GPa) would correspond to a temperature of 6700 K, which is unreasonably high even for a fully developed detonation wave (3400−4100 K).[8,31]

The next possibility, emission originating from shock induced electronic excitation of PETN, can be ruled out on the basis of the following arguments. First, emission does not appear at the instant of shock wave entry into the sample, as it would be expected for this kind of process. Second, the luminosity reaches

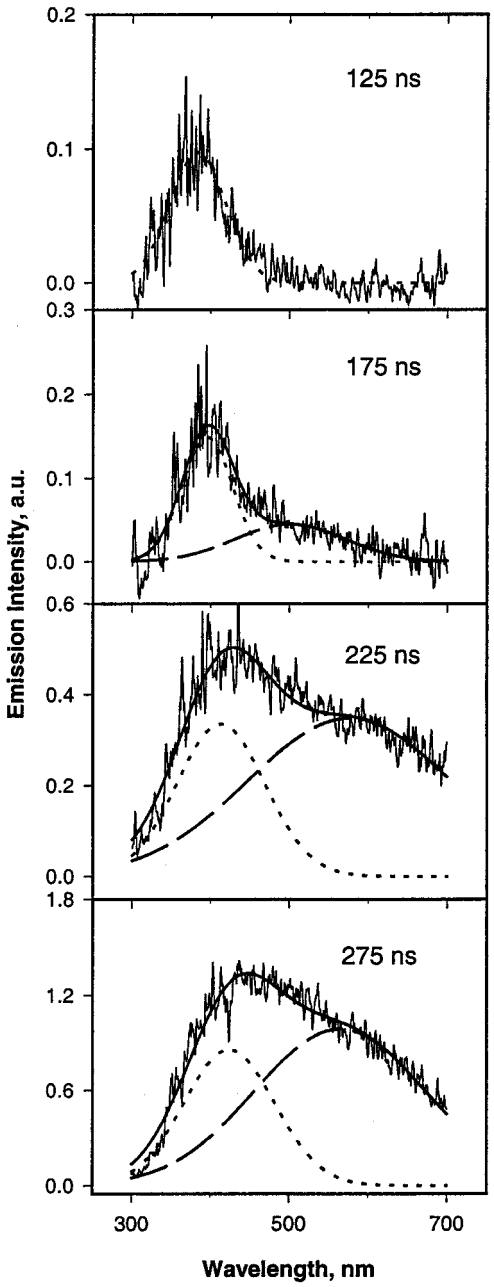

Figure 10. Evolution of emission spectrum in time for PETN shocked to 7.6 GPa along the [100] direction (experiment E2). Dashed and dotted lines correspond to the low- and high-energy components of the spectrum, respectively. Shock enters the sample at 0 ns; the spectra were collected at times shown.

its maximum after the final state has been reached and when there are no shock waves propagating in the sample. Finally, the emission spectra differ significantly from the photoluminescence spectrum of PETN. The photoluminescence has a very low quantum yield and the resulting luminosity would be very weak. Also, the maximum of the photoluminescence (~420 nm at ambient pressure) exhibits a blue shift with pressure,[32] while a red shift is observed for the shock-induced emission.

Figure 13 compares the behavior of reciprocal run distance to detonation (RDD)[4,12] to the integrated emission intensity (summed over a time interval of 800 ns) and to the reciprocal induction period for the [110] orientation. There is a clear correlation between these three quantities. In particular, all of them go through a maximum near 5 GPa (input stress). This correlation between the emission parameters and RDD suggests

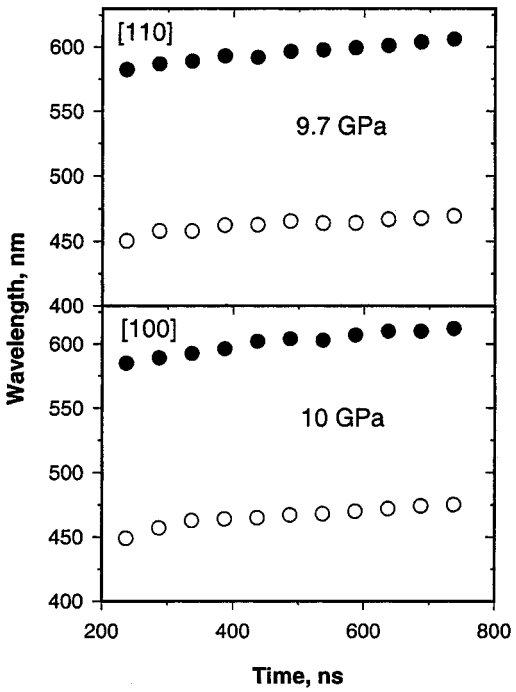

Figure 11. Position of the maxima for the low- and high-energy emission bands as a function of time. Results of experiments E6 and E1 are presented.

that the emission most likely originates from the same chemical processes that drive the shock to detonation transition. Given the above factors, the observed emission can be identified as chemiluminescence from the excited intermediates that are produced in the course of PETN decomposition.

B. Emission Components. The two components in the emission spectra separated in time and energy imply two different chemiluminescent processes. The HEB component appears first after a short induction period. Existence of the induction period suggests that the initial decomposition step is not chemiluminescent. This is reasonable because the first reaction in HE decomposition is usually rate limiting and largely endothermic, while the following reactions are relatively fast and exothermic.[33] A longer induction period for the second component indicates that either one extra step is involved in the process, giving rise to the LEB compared to the HEB, or the respective reaction is slower. However, since the LEB grows faster than the HEB, the first alternative appears to be more reasonable.

Figure 14 gives a qualitative energy diagram that is consistent with the kinetic profile just described and the expected thermochemistry of these processes. Reaction **1** is endothermic. Reaction **2** produces the first emitting intermediate. Although the combined energy of this intermediate and other reaction products cannot be determined with certainty, it is likely to be similar to that of the transition state, TS2. Therefore, it is probably higher in energy than the products of reaction **1**. Reaction **3** represents the extra step between the two emitting intermediates. It is likely exothermic and is shown as such in Figure 14. Its activation energy can either be lower than that of Reaction **2**, as shown in the figure, or higher. Reaction **4** produces the second emitting intermediate and is similar to Reaction **2**. Reactions **5** and **6** depict electronic transitions of the intermediates to the ground states producing the HEB and LEB, respectively.

Although there appears to be two chemiluminescent reactions, the number of chemiluminescing intermediates may or may not

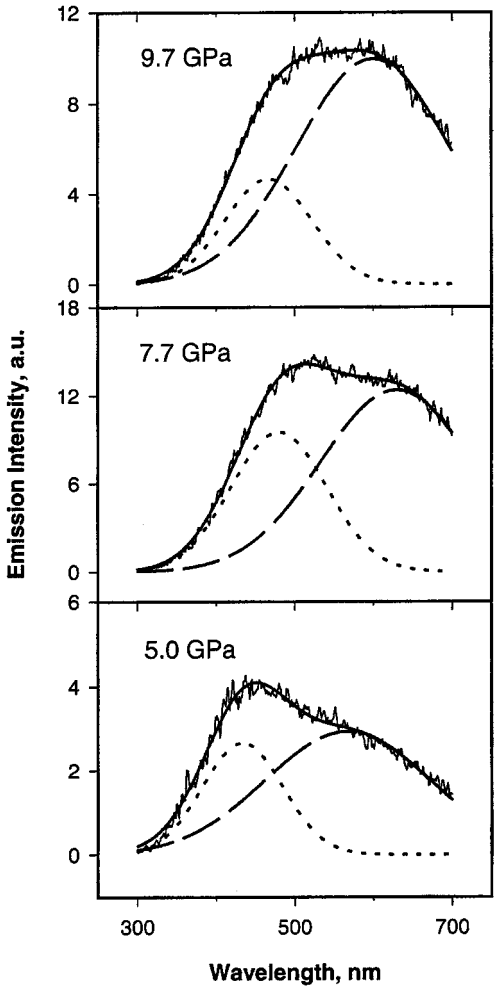

Figure 12. Stress dependence of the emission spectra for the [110] orientation. The spectra were recorded at 650 ns after the shock wave entered the sample. Dashed and dotted lines show the two components (LEB and HEB) of the spectra.

be two. In principle, it is possible that two different excited states of the same intermediate give rise to the two emission components. For this to occur, two requirements need to be satisfied: (1) the potential energy surface (PES) of each reaction must cross with the corresponding excited state of the intermediate and (2) internal conversion between the excited states must be slow compared to the radiative transition to the ground state.

C. Emitting Intermediate. It is well-known that highly exothermic reactions producing small molecules are more likely to result in chemiluminescence since the energy would be difficult to accommodate within the limited degrees of freedom of such products.[34] Therefore, it is reasonable to look for the emitting species among the small molecules expected to form in the course of PETN decomposition. Previously, nitrogen dioxide, NO_2, was tentatively suggested as the emitting species.[4] However, only the LEB is close in energy to the transition energy of nitrogen dioxide (2 eV; $X(^2A_1) \leftarrow A(^2B_2)$ transition).[35−37] The HEB cannot be explained by NO_2 because the $^2B_2$ state of NO_2 has a dissociative limit of 390 nm. This emission cutoff is not present in our experiments.

Emission from NO was suggested to account for light below 390 nm.[4] However, the NO $X(^2\Pi_{1/2}) \leftarrow B(^2\Pi_{3/2})$ transition peaks at 320−340 nm,[38] which does not match the HEB either. Also, the presence of NO in the early decomposition products would not be consistent with the ionic character of decomposition.[5]

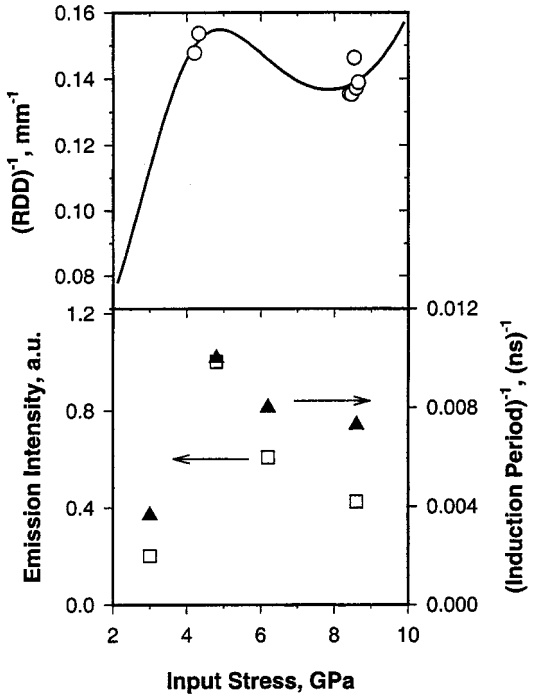

Figure 13. Correlation of run distance to detonation (RDD) and emission data (intensity and induction period) for the [110] orientation. The top panel displays RDD data of ref 6 (circles) and the solid line represents a polynomial fit to the data. The bottom panel shows total emission intensity (squares) and induction period (triangles) measured in this work.

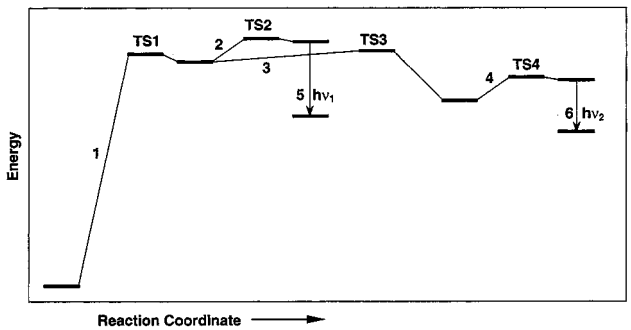

Figure 14. Qualitative energy diagram for reactions in shocked PETN. TS# denotes the transition state for each reaction. Each bold horizontal line represents either the transition state or products/intermediates formed at each decomposition step. The vertical arrows depict chemiluminescence that brings one of the species from an excited state, in which it is formed, down to the ground state. A photon is emitted in this transition. More details are given in the text.

Instead, after considering the electronic structure of NO_2^+ and analyzing it in terms of our emission data, we propose that the nitronium ion, NO_2^+, is the emitting species.

The nitronium ion is a first-row, closed-shell triatomic and is among the simplest polyatomic cations. However, the available information for NO_2^+ is limited primarily to its ground state.[39−41] To determine the electronic transition energies and geometry of the excited states we carried out ab initio calculations employing single excitation configuration interaction (CIS) and the 6-311+G(d, p) basis set implemented in Gaussian 98.[42] Figure 15 shows the PES for the ground and three lowest excited states. The ground state is linear ($^1\Sigma_g^+$) and the ON bond length is 1.122 Å.[40] In contrast, the excited states are bent; their properties are detailed in Table 2. The two lower excited states are stable as verified by vibrational analyses. The upper $^1A_2$ excited state has one imaginary frequency indicating that the

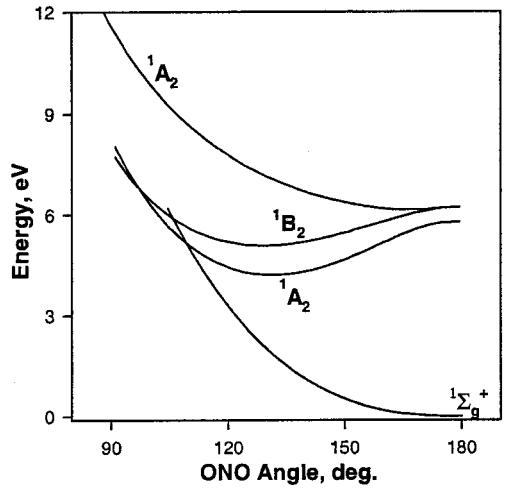

Figure 15. Electronic structure of NO_2^+. The ground state and three lowest excited states are shown.

TABLE 2: Geometry, Vibrational Frequencies, and Energy of NO_2^+ Excited States [a]

	lower $^1A_2$	$^1B_2$	higher $^1A_2$
ON length, Å	1.161	1.163	1.161
ONO angle, deg.	131.5	129.3	167.2
vibrational frequencies, cm^{-1}			
$\omega_1(B_2)$	775	627	1847
$\omega_2(A_1)$	794	810	1428
$\omega_3(A_1)$	1626	1627	870*i*
vertical-down transition, eV (nm)	2.35 (528)	2.98 (415)	

[a] CIS/6-311+G(d,p) model chemistry

state is dissociative. The cation will dissociate into $NO^+ + O$ from this state.

The vertical-up and vertical-down transitions have different transition energies by ~3 eV because of a large mismatch in the geometry of the ground and the two stable excited states. The up transitions are located in the UV while the down transitions are in the visible. For the purpose of this discussion, we will be concerned with the down transitions only. Remarkably, the transitions from the $^1B_2$ and lower $^1A_2$ states closely match the energies of the HEB and LEB, respectively. The 0.6 eV separation between the states is also in agreement with the experimental data. These findings provide the first supporting point for the identification of the nitronium ion as the emitting species.

Although the Franck−Condon principle does not strictly apply to chemical reactions, a similar constraint is expected. The geometry of the reactant will not change much during the instant when the excited state is formed. Hence, if the nuclear geometry of the transition state resembles the electronically excited product rather than its ground state, it will favor entry into the excited state.[43] The ONO angle in the PETN nitro groups is ~130°.[44,45] This value is very similar to the angles in the equilibrium geometry of both stable excited states of NO_2^+ (see Table 2). Although the molecular conformation and/or volume may be different in the transition state relative to the ground state, it is unlikely to significantly affect the ONO bond angle.[5] In contrast, this value does not conform to the linear ground state. Therefore, NO_2^+ satisfies the geometric constraints for the chemiluminescing species.

Furthermore, the emission band shifting (see Figure 11) observed in our experiments is also consistent with the expected behavior of NO_2^+. Since the decomposition mechanism is likely ionic (see section IV D), the polarity of the medium will increase as the decomposition progresses due to the formation of charged

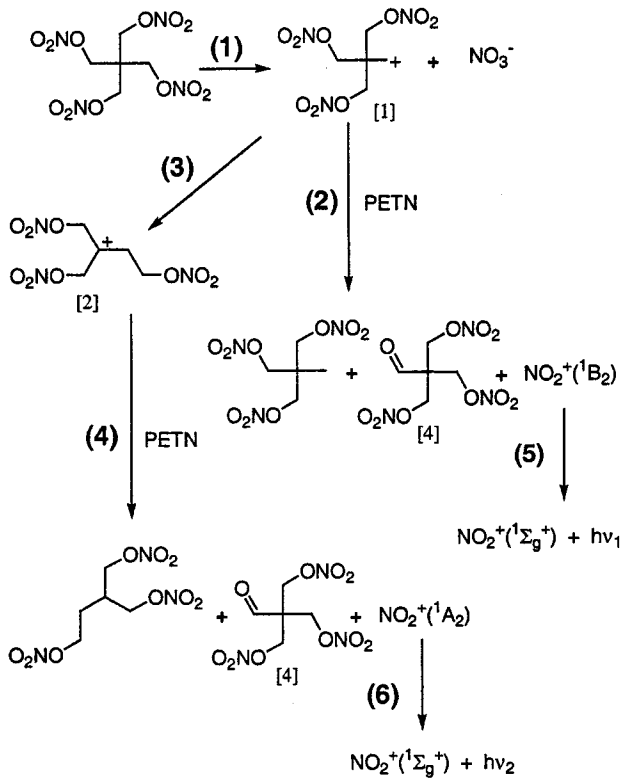

Figure 16. Proposed initiation mechanism in shocked PETN. More details are given in the text.

and polar products. This will affect transition energies through ion−ion, ion−dipole, and dipole−dipole interactions. Since the ground state of NO_2^+ is linear, it has zero dipole moment. In contrast, the excited states possess sizable dipole moments due to the bent geometry. Thus, greater energy stabilization is expected for the excited states than for the ground state. This will manifest itself as a red shift of the corresponding transitions. The transition bands are expected to maintain their separation because both states are very similar in terms of their geometry, dipole moment, and, therefore, energy stabilization.

Although there is no information available in the literature about the rate of interstate conversion in NO_2^+, some conclusions about it can be reached from the data available for the isoelectronic molecule CO_2. Chemiluminescence from CO_2 has been observed in several reactions, with the CO_2 afterglow being studied the most. The emission spectrum of CO_2 afterglow consists of two bands located at ca. 400 and 525 nm.[46] This indicates that two excited states contribute to the chemiluminescence and that the nonradiative crossing from the higher energy excited state to the lower one is slow and cannot compete with the radiative transition to the ground state. Since the electronic structures of each molecule are very similar, the same should be true for NO_2^+ as well.

These evaluations of the electronic structure, geometry, and properties of the nitronium ion are consistent with the experimental data and have led us to conclude that NO_2^+ is the chemiluminescing species. Therefore, the nitronium ion is inferred as an intermediate in the decomposition process in shocked crystalline PETN.

D. Reaction Mechanism. Given the identification of an intermediate and the qualitative reaction scheme of Figure 14, we are now in a position to propose the reaction mechanism in shocked PETN. This mechanism is shown in Figure 16.

The dominant reaction of nitrate esters at ambient pressure is homolysis of the $O-NO_2$ bond.[47] Under high pressure, a

competing reaction mechanism emerges in which the first step is the formation of a carbocation and the nitrate ion.[48−50] For PETN this is reaction **1** in Figure 16. Ionic reactions have a typical activation volume of ca. −20 cm^3/mol and, as such, they are promoted by pressure while homolysis is retarded by pressure.[51,52] The ascendancy of heterolysis over homolysis is gradual with the turning point around 0.5 GPa.[48] Although there are no direct data for PETN, it is reasonable to assume that it follows the same pattern as other nitrate esters. Therefore, the operative mechanism in PETN at stresses of ca. 5−10 GPa is likely to be ionic. Reaction **1** in the gas phase is endothermic by about 180 kcal/mol as estimated using *AM1* semiempirical calculations. The amount of endothermicity is likely to be reduced significantly in a polar environment.[5]

Carbocation [1] is a primary carbocation. As such, it is prone to rearrangement to tertiary carbocation [2] via reaction **3** in Figure 16.[53] Reaction **3** is exothermic by about 22 kcal/mol (as estimated using *AM1*). Further reactions of carbocations [1] and [2] are less certain. However, on the basis of our experimental results these reactions must yield NO_2^+. A helpful consideration here is the following reaction:

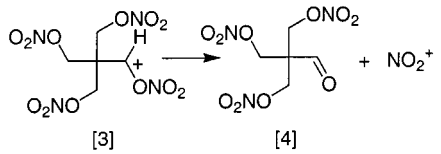

(A)

Cation [3] can be obtained via abstraction of the hydride ion, H^-, from PETN. It is unstable (IRC calculation[42]) and eliminates the nitronium ion to produce [4], the trinitrate aldehyde derivative of PETN. Both carbocations [1] and [2] can serve as hydride ion acceptors.[53] However, because of the intrinsic instability of [3], an abstraction step is likely to occur concurrently, with reaction (A) as a bimolecular reaction providing two separate pathways to NO_2^+, as shown in Figure 16 by reactions **2** and **4**.

Reactions **2** + **5** and **4** + **6** are exothermic by ca. 38 and 25 kcal/mol, respectively, (as estimated using *AM1*). To satisfy the energy balance necessary to produce excited states of NO_2^+, the transition state in these reactions must lie above the products by at least 70 and 55 kcal/mol, respectively. The latter translates into an activation energy of ∼30 kcal/mol, which is very reasonable for this type of reaction. The heats of reactions **2** + **5** and **4** + **6** are different by ∼13 kcal/mol or ∼0.6 eV. This value matches the energy separation between the emission bands and explains the presence of two emission components. The amount of energy in reaction **4** is sufficient only to populate the lowest excited state of NO_2^+. On the other hand, reaction **2** has an extra 0.6 eV available, which makes the next excited state accessible from the transition state (see also Figure 14). As discussed in the preceding section, geometric constraints and slow interstate conversion will lead to emission from both excited states. Although the amount of NO_2^+ in reacting PETN cannot be determined with certainty, it is reasonable to conclude that this strong electrophile known for its high reactivity may play an important role in the reaction growth and propagation.

Together with the results of section IV C, the scheme of Figure 16 provides an interpretation of the experimental results presented in this paper. This interpretation is self-consistent and is also consistent with the physical and chemical data available in the literature. Combining all the experimental evidence and analyses presented above, we conclude that the mechanism shown in Figure 16 best describes the decomposition process in shocked PETN crystals.

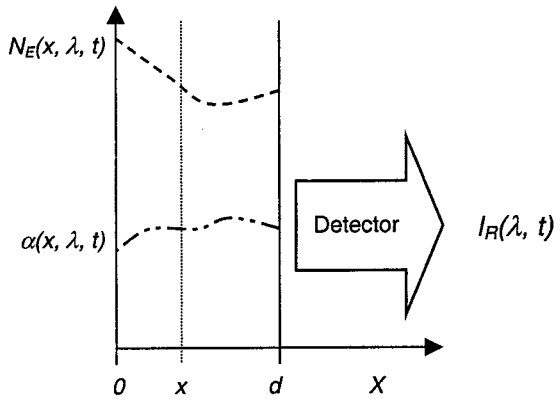

Figure 17. One-dimensional model of the experimental geometry. X is the coordinate axis and x is an arbitrary location inside the sample. The sample occupies the region from $x = 0$ to $x = d$. The detector is placed at infinity and $I_R(\lambda,t)$ is the emission intensity recorded by the detector as a function of wavelength, λ, and time, t. The dashed and dashed−dotted lines represent the distributions of the emitting and absorbing species, $N_E(x,\lambda,t)$ and $\alpha(x,\lambda,t)$, respectively.

V. Summary

Time-resolved emission spectroscopy was used to examine the decomposition mechanism in shocked PETN single crystals. PETN was shocked to peak stresses as high as 13 GPa using stepwise loading. Emission spectra were measured for thin crystalline samples shocked along two different crystallographic directions, [100] and [110].

Emission data were analyzed in conjunction with absorption data, due to the concurrent changes in the optical transmission of PETN. The absorption data were acquired separately under the same loading conditions. The raw emission data were corrected analytically by assuming spatial uniformity of the emitting/absorbing species. The applicability of this assumption was tested and verified in separate experiments. Analysis of the corrected emission data reveals two bands in the spectra: the high-energy band (HEB) at ∼3.0 eV and the low-energy band (LEB) at ∼2.4 eV. Both the HEB and LEB are observed in every experiment regardless of stress or crystal orientation. However, their relative and absolute intensities and kinetics revealed stress and orientation dependence.

The emission is identified as chemiluminescence from the nitronium ion, NO_2^+, on the basis of the electronic structure and properties of NO_2^+. Nitronium ion was analyzed using ab initio calculations, which revealed transition energies matching those of the emitting intermediate observed experimentally. Several chemical reactions compatible with the formation of NO_2^+ were considered and evaluated. Finally, a four-step chemical initiation mechanism in shocked crystalline PETN is proposed and discussed in detail.

Acknowledgment. Dr. J. M. Winey is thanked for sharing his preliminary results on the equation of state of PETN. D. Savage and K. Zimmerman are thanked for their assistance in the experimental effort. This work was supported mainly by ONR grants N000149310369 and N000149911014, and in part by DOE grant DEFG0397SF21388.

Appendix

Emission intensity recorded from a radiating object can be markedly different from the intensity actually emitted if parts of the object can reabsorb the emitted radiation. In the one-dimensional case illustrated in Figure 17, the recorded emission intensity, $I_R(\lambda,t)$, can be expressed as follows:

$$I_R(\lambda,t) = C(\lambda)\int_0^d N_E(x,\lambda,t)\, p(x,\lambda,t)\, dx \qquad (A1)$$

where $C(\lambda)$ is the spectral response of the detector; $N_E(x,\lambda,t)$ is the number of photons emitted per unit sample thickness; x is the spatial coordinate in the direction of light propagation; $p(x,\lambda,t)$ is the probability that a photon emitted from location x will be received by the detector. The latter can be expressed through the absorption coefficient, $\alpha(x,\lambda,t)$, as

$$\ln p(x,\lambda,t) = -\int_x^d \alpha(x',\lambda,t)\, dx' \qquad (A2)$$

Of physical interest, however, is the true emission intensity, $I_T(\lambda,t)$, that is unaltered by reabsorption. It can be defined as follows:

$$I_T(\lambda,t) = \int_0^d N_E(x,\lambda,t)\, dx \qquad (A3)$$

For arbitrary spatial distributions of the absorbing and emitting species, the system of eqs A1−A3 is convoluted and difficult to untangle. However, in the special case of uniform distributions, $N_E(x,\lambda,t) = N_E(\lambda,t)$ and $\alpha(x,\lambda,t) = \alpha(\lambda,t)$, it can be easily integrated. The result of this integration is given by eq 1 in the text.

References and Notes

(1) See proceedings of the *First through Eleventh Symposia (International) on Detonation*; Office of Naval Research: Arlington, Virginia, 1951−1998.

(2) Gupta, Y. M. *J. Phys. IV, Colloque,* **1995**, *5*, C4−345.

(3) Dick, J. J. *Appl. Phys. Lett.* **1984**, *44*, 859.

(4) Dick, J. J.; Mulford, R. N.; Spencer, W. J.; Pettit, D. R.; Garcia, E.; Shaw, D. C. *J. Appl. Phys.* **1991**, *70*, 3572.

(5) Gruzdkov, Y. A.; Gupta, Y. M. *J. Phys. Chem. A* **2000**, *104*, 11169.

(6) Dick, J. J., *J. Appl. Phys.* **1997**, *81*, 601.

(7) Tarver, M. C.; Breithaupt, R. D.; Kury, W. J. *J. Appl. Phys.* **1997**, *81*, 7193.

(8) Yoo, C. S.; Holmes, N. C.; Souers, P. C.; Wu, C. J.; Ree, F. H.; Dick, J. J. *J. Appl. Phys.* **2000**, *88*, 70.

(9) Halleck, P. M.; Wackerle, J. *J. Appl. Phys.* **1976**, *47*, 976.

(10) Craig, B. G. In *LASL Explosive Property Data*; Gibbs, T. R.; Popolato, A., Eds.; University of California Press: Berkeley, 1980; pp 301, 318.

(11) Soulard, L.; Bauer, F. In *Shock Compression of Condensed Matter, 1989*; Schmidt, S. C., Johnson, J. N., Davison, L. W., Eds.; Elsevier: Amsterdam, 1990; p 817.

(12) Dick, J. J.; Ritchie, J. P. *J. Appl. Phys.* **1994**, *76*, 2726.

(13) Jindal, V. K.; Dlott, D. D. *J. Appl. Phys.* **1998**, *83*, 5203.

(14) Spitzer, D.; Samirant, M. *Tenth Symposium on Detonation*; Office of Naval Research: Arlington, VA, 1993; p 831.

(15) Spitzer, D., Ph.D. Thesis, Universite Louis Pasteur de Strasbourg, 1993.

(16) Dreger, Z. A.; Gruzdkov, Y. A.; Gupta, Y. M.; Dick, J. J. In *Shock Compression of Condensed Matter, 1999*; Furnish, M. D., Chhabildas, L. C., Hixson, R. S., Eds.; AIP: New York, 2000; p 933.

(17) Dick, J. J. *J. Appl. Phys.* **1982**, *53*, 6161.

(18) Fowles, G. R.; Duvall, G. E.; Asay, J.; Bellamy, P.; Feistmann, F.; Grady, D.; Michaels, T.; Mitchell, R. *Rev. Sci. Instrum.* **1970**, *41*, 984.

(19) Gupta, Y. M. COPS code; Stanford Research Institute: Menlo Park, CA, 1976, unpublished.

(20) The *a*-axis sapphire used in this work has shown to have an elastic response nearly identical to that for the *c*-axis sapphire. The latter has been examined in Barker, L. M.; Hollenbach, R. E. *J. Appl. Phys.* **1970**, *41*, 4208.

(21) Carter, W. J. *High Temp. − High Press.* **1973**, *5*, 313.

(22) Winey, J. M., personal communication.

(23) Gruzdkov, Y. A.; Gupta, Y. M.; Dick, J. J. In *Shock Compression of Condensed Matter, 1999*; Furnish, M. D., Chhabildas, L. C., Hixson, R. S., Eds.; AIP: New York, 2000; p 929.

(24) Winey, J. M.; Gupta, Y. M. *J. Phys. Chem. A* **1997**, *101*, 9333.

(25) Gruzdkov, Y. A.; Gupta, Y. M. *J. Phys. Chem. A* **1998**, *102*, 2322.

(26) Constantinou, C. P.; Winey, J. M.; Gupta, Y. M. *J. Phys. Chem.* **1994**, *98*, 7767.

(27) Jones, S. C.; Gupta, Y. M. *J. Appl. Phys.* **2000**, *88*, 5671.

(28) Mullen, P. A.; Orloff, M. K. *J. Phys. Chem.* **1973**, *77*, 910.

(29) Kunz, A. B. *Mater. Res. Soc. Symp. Proc.* **1996**, 418, 287.

(30) Since in our experiments collection of light takes place from a small solid angle (<0.13 sr), the one-dimensional approximation employed is sufficiently accurate. The analysis presented can be easily adapted to any arbitrary direction.

(31) Mader, C. L. *Numerical Modeling of Detonation*; University of California Press: Berkeley, 1970; p 48.

(32) Dreger, Z. A.; Gupta, Y. M.; White, J. O.; Drickamer, H. G., unpublished results.

(33) Cheret, R. *Detonation of Condensed Explosives*; Springer-Verlag: New York, 1993.

(34) Gundermann, K. D.; McCapara, F. *Chemiluminescence in Organic Chemistry*; Springer-Verlag: Berlin, 1987.

(35) Hsu, D. K.; Monts, D. L.; Zare, R. N. *Spectral Atlas of Nitrogen Dioxide 5530 to 6480 Å*; Academic Press: New York, 1978.

(36) Gillespie, G. D.; Khan, A. U.; Wahl, A. C.; Hosteny, R. P.; Krauss, M. *J. Chem. Phys.* **1975**, *63*, 3425.

(37) Gillespie, G. D.; Khan, A. U. *J. Chem. Phys.* **1976**, *65*, 1624.

(38) Frosch, R. P.; Robinson, G. W. *J. Chem. Phys.* **1964**, *41*, 367.

(39) Bryant, G.; Jiang, Y.; Grant, E. *Chem. Phys. Lett.* **1992**, *200*, 495.

(40) Lee, T. J. *Chem. Phys. Lett.* **1992**, *188*, 154.

(41) Lee, T. J.; Rice, J. E. *J. Phys. Chem.* **1992**, *96*, 650.

(42) Frisch, M. J.; Trucks, G. W.; Schlegel, H. B.; Scuseria, G. E.; Robb, M. A.; Cheeseman, J. R.; Zakrzewski, V. G.; Montgomery, J. A., Jr.; Stratmann, R. E.; Burant, J. C.; Dapprich, S.; Millam, J. M.; Daniels, A. D.; Kudin, K. N.; Strain, M. C.; Farkas, O.; Tomasi, J.; Barone, V.; Cossi, M.; Cammi, R.; Mennucci, B.; Pomelli, C.; Adamo, C.; Clifford, S.; Ochterski, J.; Petersson, G. A.; Ayala, P. Y.; Cui, Q.; Morokuma, K.; Malick, D. K.; Rabuck, A. D.; Raghavachari, K.; Foresman, J. B.; Cioslowski, J.; Ortiz, J. V.; Baboul, A. G.; Stefanov, B. B.; Liu, G.; Liashenko, A.; Piskorz, P.; Komaromi, I.; Gomperts, R.; Martin, R. L.; Fox, D. J.; Keith, T.; Al-Laham, M. A.; Peng, C. Y.; Nanayakkara, A.; Gonzalez, C.; Challacombe, M.; Gill, P. M. W.; Johnson, B.; Chen, W.; Wong, M. W.; Andres, J. L.; Gonzalez, C., Head-Gordon, M.; Replogle, E. S.; Pople, J. A. *Gaussian 98, Revision A.7*, Gaussian, Inc.: Pittsburgh, PA, 1998.

(43) Rauhut, M. M. *Acc. Chem. Res.* **1969**, *2*, 80.

(44) Cady, H. H.; Larson, A. C. *Acta Crystallogr. B* **1975**, 31, 1864.

(45) Gruzdkov, Y. A.; Gupta, Y. M. *J. Phys. Chem. A* **2001**, 105, 6197.

(46) Gundermann, K. D.; McCapra, F. *Chemiluminescence in Organic Chemistry*; Springer-Verlag: Berlin, 1987; p 75.

(47) Hiskey, M. A.; Brower, K. R.; Oxley, J. C. *J. Phys. Chem.* **1991**, *95*, 3955.

(48) Naud, D. L.; Brower, K. R. *J. Org. Chem.* **1992**, *57*, 3303.

(49) Davis, L. L.; Brower, K. R. *J. Phys. Chem.* **1996**, *100*, 18775.

(50) Davis, L. L. *Reactions of Organic Compounds in Explosive-Driven Shock Waves*; Ph.D. Dissertation, New Mexico Institute of Mining and Technology, 1996.

(51) Asano, T.; le Noble, W. J. *Chem. Rev.* **1978**, *78*, 407.

(52) Klarner, F. G.; Diedrich, M. K.; Wigger, A. E. In *Chemistry under Extreme or Non-Classical Conditions*; van Eldik, R., Hubbard, C. D., Eds.; Wiley: New York, 1997; p 103.

(53) Morrison, R. T.; Boyd, R. N. *Organic Chemistry*, 5th ed.; Allyn and Bacon: Boston, 1987; Chapters 5, 6, and 7.